Available online at www.sciencedirect.com
ScienceDirect
Marine Pollution Bulletin 54 (2007) 1207–1211
MARINE POLLUTION BULLETIN
www.elsevier.com/locate/marpolbul

Marine debris collects within the North Pacific Subtropical Convergence Zone

William G. Pichel [a], James H. Churnside [b,*], Timothy S. Veenstra [c], David G. Foley [d,e], Karen S. Friedman [a], Russell E. Brainard [f], Jeremy B. Nicoll [g], Quanan Zheng [h], Pablo Clemente-Colón [a]

[a] National Oceanic and Atmospheric Administration (NOAA), National Environmental Satellite, Data, and Information Service, Room 102 WWB, 5200 Auth Road, Camp Springs, MD 20746, USA
[b] NOAA, Earth System Research Laboratory, 325 Broadway, Boulder, CO 80305, USA
[c] Airborne Technologies Inc., 4338 N. Gunflint Trail, Wasilla, AK 99654, USA
[d] Joint Institute for Marine and Atmospheric Research, University of Hawaii, USA
[e] NOAA Southwest Fisheries Science Center, Environmental Research Division, 1352 Lighthouse Ave., Pacific Grove, CA 93950, USA
[f] NOAA Pacific Islands Fisheries Science Center, 2570 Dole Street, Honolulu, HI 96822, USA
[g] Alaska Satellite Facility, Geophysical Institute, University of Alaska Fairbanks, P.O. Box 757320, Fairbanks, AK 99775, USA
[h] Department of Atmospheric and Oceanic Science, University of Maryland, College Park, MD 20742, USA

Abstract

Floating marine debris, particularly derelict fishing gear, is a hazard to fish, marine mammals, turtles, sea birds, coral reefs, and even human activities. To ameliorate the economic and environmental impact of marine debris, we need to efficiently locate and retrieve dangerous debris at sea. Guided by satellite-derived information, we made four flights north of Hawaii in March and April 2005. During these aerial surveys, we observed over 1800 individual pieces of debris, including 122 derelict fishing nets. The largest debris concentrations were found just north of the North Pacific Transition Zone Chlorophyll Front (TZCF) within the North Pacific Subtropical Convergence Zone (STCZ). Debris densities were significantly correlated with sea-surface temperature (SST), chlorophyll-*a* concentration (Chl*a*), and the gradient of Chl*a*. A Debris Estimated Likelihood Index (DELI) was developed to predict where high concentrations of debris would be most likely in the North Pacific during spring and early summer.

Keywords: Marine debris; Derelict fishing gear; North Pacific Subtropical Convergence Zone

1. Introduction

The increased use of long-lasting synthetic materials since the 1950s has led to increases in the negative effects of marine debris. Plastic particles are ingested by sea birds and small marine animals instead of food (Carr, 1987). Fish, birds, sea turtles, and marine mammals are entangled and killed in derelict nets (also referred to as "ghostnets") (Laist, 1987). Ships and submersibles can be trapped by the fouling of nets and lines in propellers or damaged by collision with bulky floating debris. Nets physically damage coral reef substrates while they continue to entangle and kill reef animals (Donohue et al., 2001). Between 1996 and 2006, NOAA recovered a total of 511 metric tons of fishing gear from the reefs of the Northwest Hawaiian Island Marine National Monument (NWHI-MNM), one of the largest marine conservation areas in the world. A recent report estimates an annual accumulation rate of approximately 52 metric tons of derelict fishing gear (Dameron et al., 2006). The economic loss of commercial

* Corresponding author. Tel.: +1 303 497 6744.
E-mail address: james.h.churnside@noaa.gov (J.H. Churnside).

0025-326X/$ - see front matter © 2007 Elsevier Ltd. All rights reserved.
doi:10.1016/j.marpolbul.2007.04.010

fish caught in ghostnets; the time and expense of rescue operations for entangled or damaged vessels; the environmental loss of endangered species and rare coral; and the cost of cutting nets by hand from reefs can be measured in millions of dollars annually in the US alone. To mitigate some of these effects, we pursued the development of a procedure to economically locate and cost effectively remove derelict nets at sea, prior to much of the environmental damage.

Ocean circulation models, satellite remote sensing data, and aircraft observations were used to detect derelict nets and other debris in the open ocean. Ocean circulation models indicated surface convergence in the vicinity of the STCZ north of the Hawaiian Islands. Satellite remote sensing data, including wind stress, SST, and Chl*a*, indicated specific areas within the STCZ where higher concentrations of debris might be expected. Aerial surveys, based on these data, provided the distribution of the density of marine debris of several types.

Ocean circulation and wind-drift models suggest that debris in the North Pacific would tend to concentrate along a southwest-to-northeast line north of the Hawaiian Islands (Kubota, 1994) that coincides with the STCZ (Fig. 1). In the central North Pacific, the STCZ is located between 23°N and 37°N, seasonally migrating between these extremes (Roden, 1975), and marks the boundary between the productive waters of the North Pacific Transition Zone and the oligotrophic waters to the south. In general, the STCZ is located along the axis of the North Pacific high pressure ridge between the mid-latitude westerlies and the easterly trade winds, and convergence is caused by Ekman transport (Roden, 1975).

The TZCF migrates throughout the year, with its northernmost position in summer and southernmost in winter. Interannual climate signatures, such as El Niño Southern Oscillation, influence the TZCF. For example, during El Niño years, the southernmost position of the TZCF is generally further to the south than in normal years. Fig. 2 is a time series of the TZCF position as tracked by the 0.2 mg/m^3 Chl*a* isopleth and the 18 °C isotherm, both of which usually coincide with the TZCF (Bograd et al., 2004). Chlorophyll measurements are from the Sea-viewing Wide Field-of-view Sensor (SeaWiFS) on the OrbView-2 satellite and SST measurements are from the Advanced Very High Resolution Radiometer (AVHRR) on the NOAA series of polar-orbiting operational environmental satellites. Both were derived from a time series of 8 day averages between 160°W and 180°W. The background shows the wind stress curl calculated from satellite scatterometers (the Advanced Microwave Instrument on the ERS-2 spacecraft and Seawinds on the QuikSCAT spacecraft). The wintertime position of the TZCF coincides with the region of maximum negative wind stress curl (i.e., maximum convergence from wind-driven Ekman drift) (Bograd et al., 2004).

Thus, we expected that marine debris would be concentrated during winter when the surface convergence is strongest. Since the same winds that create the strong convergence make aerial observations of the ocean surface difficult, the best time to search for debris should be in the spring, when calmer weather occurs in the region of maximum wintertime convergence, and before the debris has

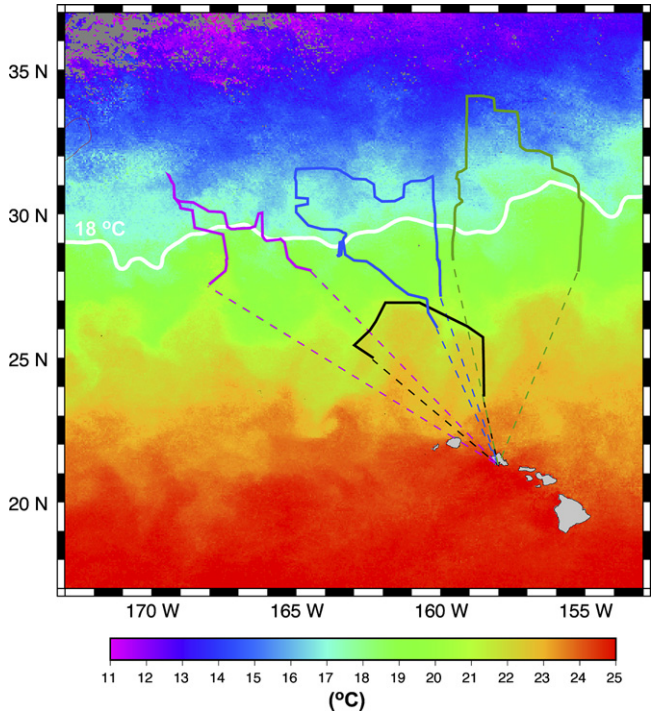

Fig. 1. 14-Day SST GOES composite for the period ending March 31, 2005 with the four GhostNet flight tracks superimposed. (Flight 1, March 18 – black; Flight 2, March 27 – red violet; Flight 3, March 29 – green; Flight 4, April 3 – blue).

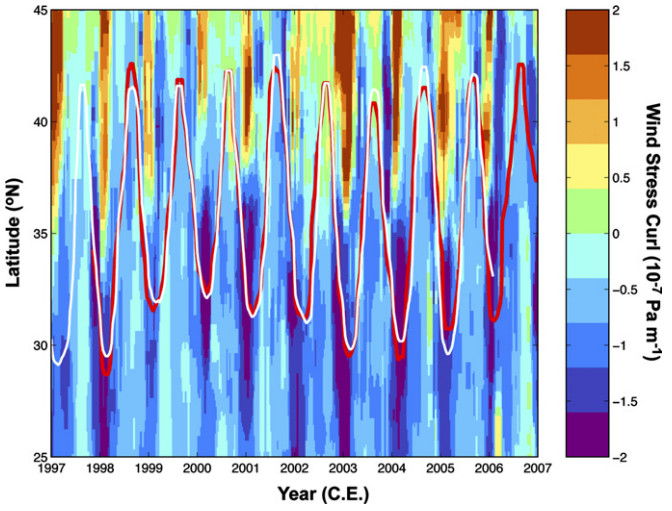

Fig. 2. Time series of Chl*a* and SST fronts, defined by the 0.2 mg m^{-3} isopleth (red line) and the 18 °C isotherm (white line), respectively. The background is wind stress curl (negative indicates convergence).

had time to disperse. For these reasons, we made a series of aerial surveys in the spring of 2005.

2. Methods

We made four flights (Fig. 1) out of Honolulu, Hawaii between March 18, 2005 and April 3, 2005 on a Lockheed WP-3D. A short test flight was followed by three flights of roughly 9 h each. During the observation periods, the flight altitude was 300 m and the speed was about 100 m s^{-1}. The flight tracks were chosen to include areas of high SST and Chl*a* gradients and also regions of low gradients, based on multi-day composites of satellite-derived SST and Chl*a* for January through March. We also used meteorological forecasts to avoid high winds (>15 m s^{-1}), since rough seas make visual observations difficult.

Four to six people made visual observations and reported them over the aircraft intercom system to a recorder, who wrote down all observations within each 1-minute period. Most sightings were first made by one or both pilots. An experienced observer at a window behind the cockpit on each side of the cabin confirmed the pilot sightings and occasionally added sightings that were missed by the pilots. Periodically, 1 or 2 additional observers near the rear of the cabin checked the performance of the primary observers.

After the flights, the density of debris was estimated for each 6 min flight period using the speed of the aircraft and an effective width of the visual survey of 1000 m. This width was estimated from geometric measurements of visibility from the aircraft windows made on the ground and from angular measurements of some of the sightings that were made during flight.

Satellite data at the positions of the debris-density estimates were extracted from 14-day composite images of Chl*a* concentration and SST. These were obtained from the MODIS/Aqua and the infrared imager on the NOAA Geostationary Operational Environmental Satellite (GOES-10), respectively. The spatial resolution of the SST data set was 0.05 by 0.05°, while that of the Chl*a* data was 0.025 by 0.025°. We also calculated the magnitude of the gradients of chlorophyll and SST to get a total of four geophysical parameters. These gradients were calculated using adjacent 0.05° resolution elements, and the longitudinal gradients were adjusted by the cosine of the latitude. These four geophysical parameters were binned by value using the following bin widths: SST – 0.5 °C; SST gradient – 0.25 °C per degree of latitude; Chl*a* – 0.025 mg m^{-3}; and Chl*a* gradient – 0.015 mg m^{-3} per degree of latitude.

The total number of debris sightings corresponding to each bin of each of the geophysical parameters was divided by the time spent searching in water with that parameter to obtain a measure of debris per unit effort (DPUE) for each parameter.We fit each DPUE to a fourth-order polynomial. Finally, we defined a Debris Estimated Likelihood Index (DELI) as the product of the DPUEs for SST, Chl*a*, and Chl*a* gradient, normalized by the largest value of this product.

3. Results

The total numbers of objects observed are presented by type in Table 1. By far, the most common form of debris was fishing floats, typically foam "corks" and plastic buoys. Less common were large net bundles, but some of these were very large (two were greater than 10 m in diameter). The category "general debris" includes plastic bags, pails, and any other miscellaneous debris.

Fig. 3 presents the observed debris densities for Flights 2, 3 and 4 (Flight 1 was a test and calibration flight). Here the 6 min totals for debris sightings have been displayed as debris density (number of sightings per km^2) superimposed on a background of Chl*a* inferred from the Moderate Resolution Imaging Spectroradiometer (MODIS) on the NASA Aqua satellite for the 14-day period spanning the time period of the flights. One can clearly see a large increase in debris density in the regions of higher chlorophyll (above the TZCF with chlorophyll equal to or greater than 0.2 mg m^{-3} – in general the orange and red regions in Fig. 3). It should be noted, however, that a number of nets were sighted south of 30°N on the western leg of Flight 3 and the eastern leg of Flight 4 (which were close in longitude to each other). This may mark an area of convergence in the past, a "fossil front" (Roden, 1980) with debris still resident.

The distribution of debris density by environmental parameter is presented in Fig. 4. The densities are averaged over 6 min sections of the flights (36 km^2). The figure also includes a least-squares fit of a fourth-order polynomial to each distribution. The dashed, cyan lines represent the prediction error estimate. They represent one standard deviation above and below the fit, based on a covariance matrix

$$\mathbf{C} = \mathbf{R}'\mathbf{R}'^{\mathrm{T}}\|\mathbf{r}\|^2/n, \tag{1}$$

where $\mathbf{R}'$ is the inverse of the Cholesky factor $\mathbf{R}$ from a QR decomposition of the Vandermonde matrix of the fit (Press et al., 1992), the superscript T represents the transpose of that matrix, n is the number of degrees of freedom, and $\|\mathbf{r}\|$ is the norm of the residuals.

Table 1
Debris totals by category

Debris type	Flight 2	Flight 3	Flight 4	Total
Buoys	24	31	13	68
General debris	29	86	158	273
Floats	201	560	631	1394
Lines	1	9	13	23
Logs	4	2	1	7
Nets	20	43	59	122
Total	279	731	875	1885

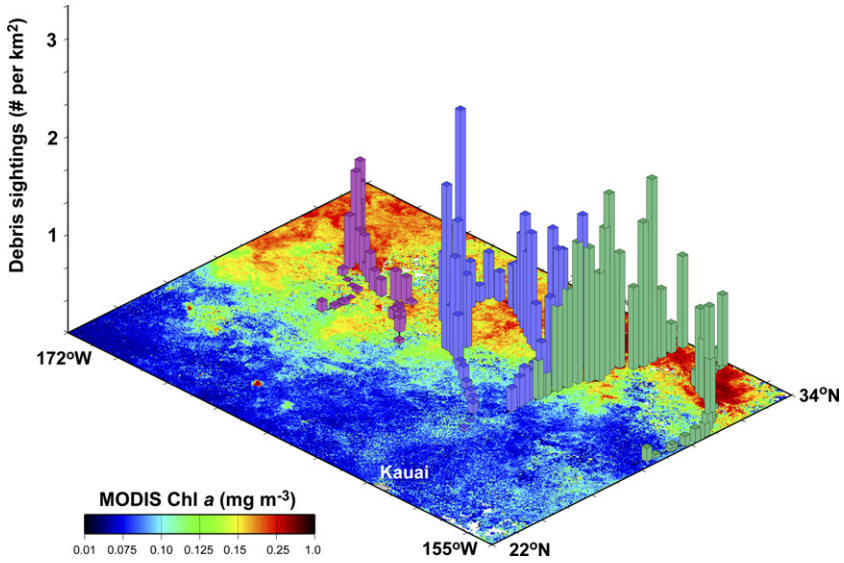

Fig. 3. Debris density for GhostNet flights 2 (red violet), 3 (green), and 4 (blue) over a background of Chl*a*.

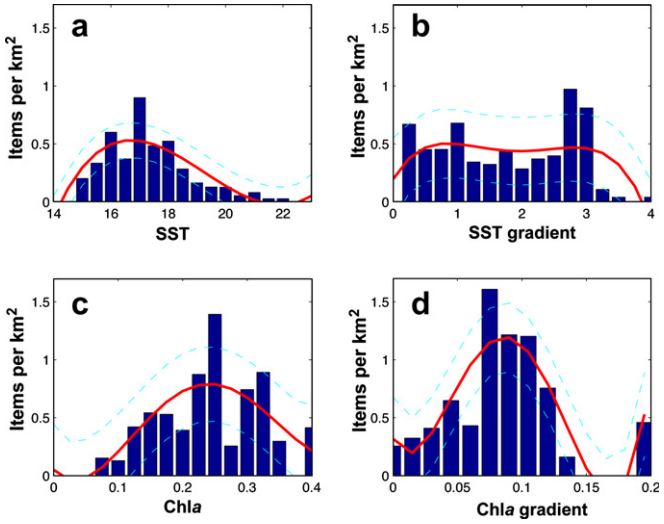

Fig. 4. Distribution of debris density by environmental parameter, along with the fourth-order polynomial fit (red line) and the lines representing ±1 standard deviation (cyan).

There was a strong correlation between the density of debris and the geophysical parameters, but this was partly because we concentrated our search in areas where we expected to find debris based on the satellite observations. After removing this effect through the calculation of the amount of debris per unit effort (DPUE), we obtained correlations of 0.87 ($n = 1832$, $p < 0.0001$) with SST, 0.61 ($n = 1832$, $p = 0.01$) with SST gradient, 0.76 ($n = 1630$, $p = 0.0005$) with Chl*a*, and 0.90 ($n = 1550$, $p < 0.0001$) with Chl*a* gradient. Since we observed significant correlations between debris density and three of the geophysical parameters, we developed a method to combine these parameters into a measure of the relative likelihood of encountering concentrations of marine debris, the Debris Estimated Likelihood Index (DELI). This produces a map (Fig. 5) that can be used to direct future aerial searches, and can also be used as a starting point for an estimate of the total amount of debris in the North Pacific. This map clearly shows that there are very localized regions of high likelihood. As derived, the DELI map is valid only for spring and early summer. As the convergence moves north, it will weaken and debris will begin to disperse from the early summer positions.

We also recorded animal sightings, including birds, dolphins, whales, turtles, and fish (Table 2). No attempt was made to get more detailed information than presented. The largest category is dolphins, but this included one group of several hundred animals. For our comparison,

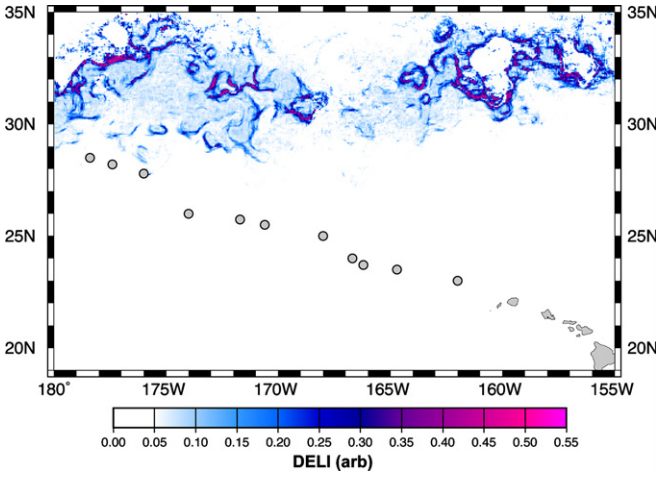

Fig. 5. Debris Estimated Likelihood Index (DELI) with relative likelihood of finding debris indicated by color. Gray denotes Hawaiian Islands, with circles at the locations of reefs too small to be resolved.

Table 2
Animal sightings by type

Animal type	Flight 2	Flight 3	Flight 4	Total
Birds	65	32	46	143
Turtles	1	0	1	2
Whales	1	0	19	20
Dolphins	0	0	256	256
Fish	0	4	3	7
Total	67	36	325	428

we used 250 animals, but the actual number could be anywhere between 200 and 300. Without this group, there were more birds than any other type. Many of these were clearly albatross, but most were not identified. The fish that could be identified were all sharks.

The overall correlation between animal sightings and debris sightings was only 0.19 ($n = 150$, $p = 0.02$). However, this low correlation was strongly influenced by a group of several hundred dolphins that were travelling in the area. If we remove these animals from the data set, the correlation improves to 0.75 ($n = 149$, $p < 0.0001$). We conclude that the pelagic animals we observed were preferentially foraging in the same convergence zones that concentrate marine debris, thus increasing their risk (Polovina et al., 2001; Seki et al., 2002).

4. Conclusions

The challenge was to develop a cost-effective method to search the vast ocean. Such a method has been found for the North Pacific. From ocean circulation models, we know that the highest concentration of debris will be concentrated in the STCZ in the spring and early summer. We have shown that aerial surveys can be localized within the STCZ using satellite-derived information about SST and Chl*a*.

The data collected during the aerial surveys support the hypothesis of a substantial increase in the rate of debris deposition on the reefs of the recently established Northwestern Hawaiian Islands Marine National Monument (NWHI-MNM) in winter and early spring when the TZCF moves south into the islands. They also suggest that a variety of marine animals tend to be concentrated in the same areas as marine debris.

Acknowledgements

The authors acknowledge the expertise and dedication of the pilots, crew, and support personnel of the NOAA Aircraft Operations Center; the assistance of those who served as observers on the flights; the insight provided by James Ingraham and his drift model studies of debris circulation in the Pacific; Michael Van Woert for his insights concerning the subtropical convergence zone; Capt. Charles Moore for sharing his experience with actual debris observations at sea. The NOAA CoastWatch program provided the GOES SST data; the NASA Goddard Space Flight Center (GSFC) provided the MODIS satellite data; the NOAA National Oceanographic Data Center provided the Pathfinder SST data; GSFC and Orbimage Inc. provided SeaWiFS Chlorophyll *a* data; and the French Institute for the Research and Exploitation of the Sea (IFREMER) provided the scatterometer wind data. The views, opinions, and findings contained in this report are those of the authors and should not be construed as an official National Oceanic and Atmospheric Administration or US Government position, policy, or decision.

References

Bograd, S.J., Foley, D.G., Schwing, F.B., Wilson, C., Laurs, R.M., Polovina, J.J., Howell, E.A., Brainard, R.E., 2004. On the seasonal and interannual migrations of the transition zone chlorophyll front. Geophysical Research Letters 31 (L17204), 1–5. doi:10.1029/2004GL02063.

Carr, A., 1987. Impact of nondegradable marine debris on the ecology and survival outlook of sea turtles. Marine Pollution Bulletin 18, 352–356.

Dameron, O.J., Parke, M., Albins, M.A., Brainard, R., Marine debris accumulation in the Northwestern Hawaiian Islands: an examination of rates and processes. Marine Pollution Bulletin. doi:10.1016/j.marpolbul.2006.11.019.

Donohue, M., Boland, R.C., Sramek, C.M., Antonelis, G.A., 2001. Derelict fishing gear in the Northwestern Hawaiian Islands: diving surveys and debris removal in 1999 confirm threat to coral reef ecosystems. Marine Pollution Bulletin 42, 1301–1312.

Kubota, M., 1994. A mechanism for the accumulation of floating marine debris north of Hawaii. Journal of Physical Oceanography 24, 1059–1064.

Laist, D.W., 1987. Overview of the biological effects of lost and discarded plastic debris in the marine environment. Marine Pollution Bulletin 18, 319–326.

Polovina, J.J., Howell, E., Kobayashi, D.R., Seki, M.P., 2001. The transition zone chlorophyll front, a dynamic global feature defining migration and forage habitat for marine resources. Progress in Oceanography 29, 469–483.

Press, W.H., Teukolsky, S.A., Vetterling, W.T., Flannery, B.P., 1992. Numerical Recipes in C: The Art of Scientific Computing, second ed. Cambridge University Press, Cambridge, pp. 96–102.

Roden, Gunnar, 1975. On North Pacific temperature, salinity, sound velocity and density fronts and their relation to the wind and energy flux fields. Journal of Physical Oceanography 5, 557–571.

Roden, Gunnar, 1980. On the subtropical frontal zone north of Hawaii during winter. Journal of Physical Oceanography 10, 342–362.

Seki, M.P., Polovina, J.J., Kobayashi, D.R., Bidigare, R.R., Mitchum, G.T., 2002. An oceanographic characterization of swordfish (*Xiphias gladius*) longline fishing grounds in the springtime subtropical North Pacific. Fisheries Oceanography 11, 251–266.